Heliyon 8 (2022) e09163

Contents lists available at ScienceDirect

Heliyon

journal homepage: www.cell.com/heliyon

Research article

Structure and biological activity of particles produced from highly activated carbon adsorbent

Veronika Sarnatskaya [a], Yuliia Shlapa [b,*], Alexandra Lykhova [a], Olga Brieieva [a], Igor Prokopenko [a], Alexey Sidorenko [a], Serhii Solopan [b], Denis Kolesnik [a], Anatolii Belous [b], Vladimir Nikolaev [a]

[a] *Kavetsky Institute of Experimental Pathology, Oncology and Radiobiology, National Academy of Sciences of Ukraine, Ukraine*
[b] *V. I. Vernadsky Institute of General and Inorganic Chemistry of the NAS of Ukraine, 32/34, Palladina Ave., Kyiv, 03142, Ukraine*

GRAPHICAL ABSTRACT

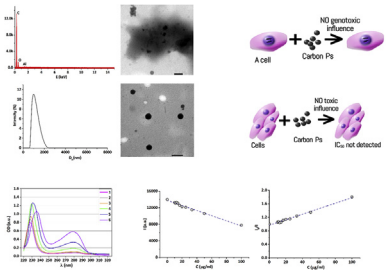

ARTICLE INFO

Keywords:
Carbon particles
BSA conformation
Cytotoxicity
Genotoxicity

ABSTRACT

Over the recent years, carbon particles have gained relevance in the field of biomedical application to diminish the level of endo-/exogenous intoxication and oxidative stress products, which occur at different pathological states. However, it is very important that such carbon particles, specially developed for parenteral administration or *per oral* usage, possess a high adsorption potential and can remove hazard toxic substances of the hydrophilic, hydrophobic and amphiphilic nature usually accumulated in the blood due to the disease, and be absolutely safe for normal living cells and tissues of organism. In this work, the stable monodisperse suspension containing very small-sized (D_{hydro} = 1125.3 ± 243.8 nm) and highly pure carbon particles with an excellent accepting ability were obtained. UV-spectra, fluorescence quenching constant and binding association constant were provided by the information about conformational alterations in an albumin molecule in presence of carbon particles, about the dynamic type of quenching process and low binding affinity between carbon and protein. The later was confirmed by DSC method. *In vitro* cell culture experiments showed that carbon particles did not possess any cytotoxic effect towards all testing the normal cell lines of different histogenesis, did not show genotoxic effects and were absolutely safe for experimental animals during and after their parenteral administration. These observations may provide more information about how to develop a safe preparation of carbon particles for different biomedical applications, in particular, as a mean for intracorporeal therapy of various heavy diseases accompanied by the increased endogenous intoxication and the level of oxidative stress.

* Corresponding author.
E-mail address: yuliashlapa@ukr.net (Y. Shlapa).

https://doi.org/10.1016/j.heliyon.2022.e09163
Received 21 August 2021; Received in revised form 12 November 2021; Accepted 17 March 2022

1. Introduction

The positive effects of modern methods of sorption therapy, such as direct hemoperfusion (DHP), per oral usage of carbon materials – enterosorption, and application-sorption therapy can be associated not only with the direct removal of toxic substances from the body during the procedure, but also with the entry into the bloodstream a certain amount of nano- and micro (1-2μ) - sized particles of activated carbon. The reason for the appearance of these particles in body fluids may be associated with their leaching from the surface by carbon hemosorbents, the spectrum of which is practically impossible to control according to the strict standards of the British (BP) and American (USP) Pharmacopoeias. Being in the intestine lumen, particles of carbon enterosorbent can pass through its walls and enter the bloodstream. Direct contact of the carbon dressing with the wound surface promotes the flow of carbon particles into the lesion focus and blood.

Entering the carbon particles into the body can be associated with prolonged positive modification of natural progression of certain diseases, in respect of which the hemoadsorption onto carbon adsorbent often promotes the intensification and acceleration of regenerative processes in the affected organs and tissues [1], as well as enterosorption and application of carbon adsorption fibrous materials for the treatment of wounds and burns - also possess the similar manifestations and consequences [2].

Carbon particles include: single- and double - wall carbon nanotubes, fullerenes, nanodiamonds, etc. Currently, there is an extensive literature describing the positive effects of carbon particles or their composites, their ability to act as scavengers of free radicals caused by the development of oxidative stress, and to mimic the properties of some enzymes belonging to the antioxidative defense system of organism. Sandhir R. et al believe that such antioxidants have a powerful potential for relieving manifestations and consequences of the oxidative stress and have serious prospects for their application [3]. For example, nanoparticles (NPs) (diameter near 50 nm) on the base of composite of fullerenes C60 (OH) 10 and 2-hydroxypropyl-β-cyclodextrin (HP-β-CD) showed positive action as the suppressors of oxidative stress, and acted as the life-span prolongers of experimental animals with fulminant hepatitis induced by the paracetamol injection [4]. Carbon clusters functionalized with PEG showed their selective accumulation in the mitochondria of T-lymphocytes, and demonstrated the effective absorption of the active oxygen species and hydroxyl radicals [5].

Numerous studies of carbon particles usage in the field of experimental oncology are currently underway. Arifa RD et al demonstrated that carbon nanocomposite reduced the degree of leukopenia and intensity of intestinal damage caused by cytostatic Irinotecan but not effected on its antitumor activity [6]. The same nanocomposite also reduced the lethality of mice with acute reaction "transplant against host", promoted osteogenesis of stem cells originated from adipose tissue [7, 8]. Fullerenol C_{60} $(OH)_{24}$ mitigated to some extent the morphological picture of the damaged heart muscle caused by anticancer antibiotic doxorubicin [9], protected renal, testicular and lung tissue in rats against oxidative stress caused by the administration of doxorubicin [10]. Andrievsky GV et al demonstrated a significant radioprotective effect of hydrophilized fullerenes in the X-ray irradiation of mice in a lethal dose of 7 Gr [11]. Derivatives of fullerenes effectively accelerated the healing lesions, including scratches and skin irritations [12]. Fullerenes coated with the polyvinylpyrrolidone demonstrated suppression of melanogenesis induced by the ultraviolet irradiation of the skin [13]. The single-walled carbon nanotubes connected to iron oxide proved to be a promising carrier for doxorubicin and tumor-specific antibodies [14, 15] as well as synthesized magnetic Fe_3O_4 particles in the shell of partially graphitized carbon demonstrated their high peroxidase-like activity in the decomposition of H_2O_2 leading to the formation of highly active hydroxyl radicals [16]. Besides that, graphene - iron oxide composite demonstrated the synergistic antibacterial effect of local heating on the culture of metacycline-resistant *Staphylococcus aureus* [17]. The authors [18], based on the literature data and the large-scale results of their own studies, put forward a hypothesis about the possible use of carbon dots as monotherapy or combination therapy for patients with malignant neoplasms.

It should be noted that the most described in literature positive effects were caused by carbon particles of different origins, which possess a very modest sorption capacity and belong to the category of nanoparticles, i.e.

Table 1. Experimental scheme of investigation of in vivo toxicity of CPs.

Group	Dose (mg/kg)	Number of animals	Cumulative dose (mg/kg)
I	0.2	5	2.8
II	0.4	5	5.6
III	1.6	5	22.4
IV	2.56	5	35.8

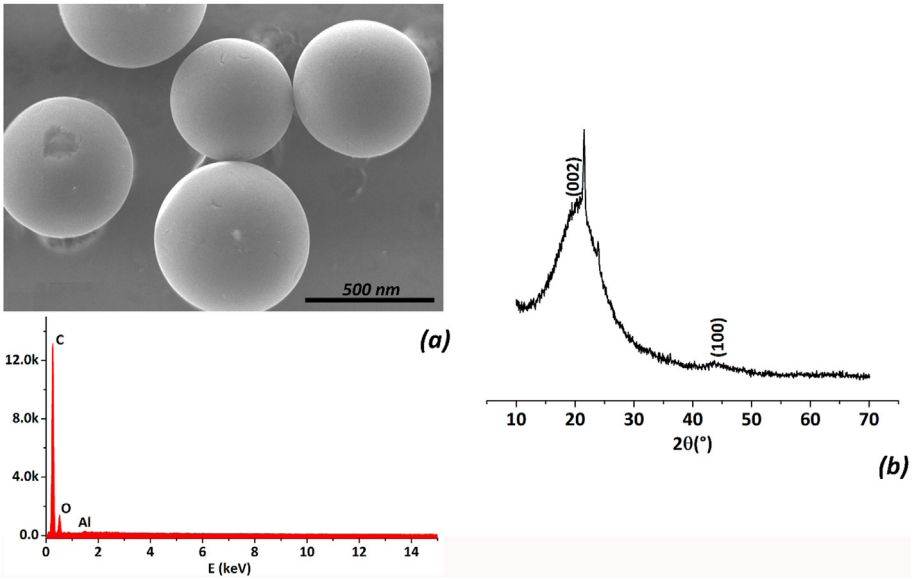

Figure 1. Representative SEM-image and EDX spectrum of the initial carbon beads (a) and XRD pattern of obtained CPs (b).

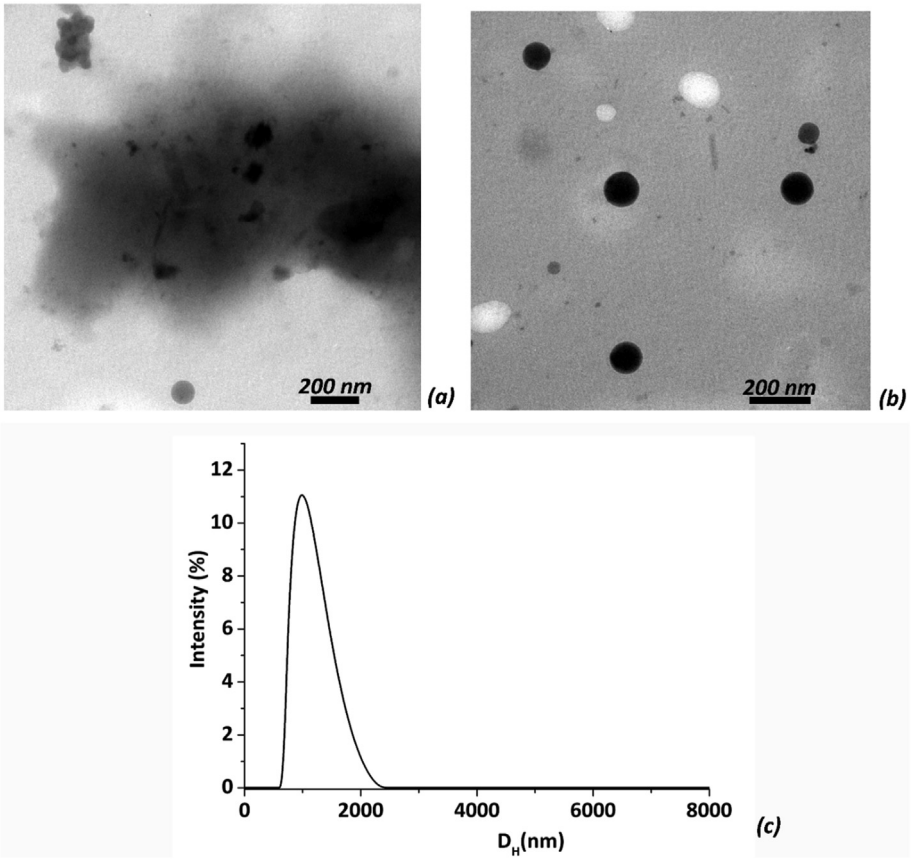

Figure 2. Representative TEM images of carbon particles (a, b) and their hydrodynamic diameter measured via DLS method (c).

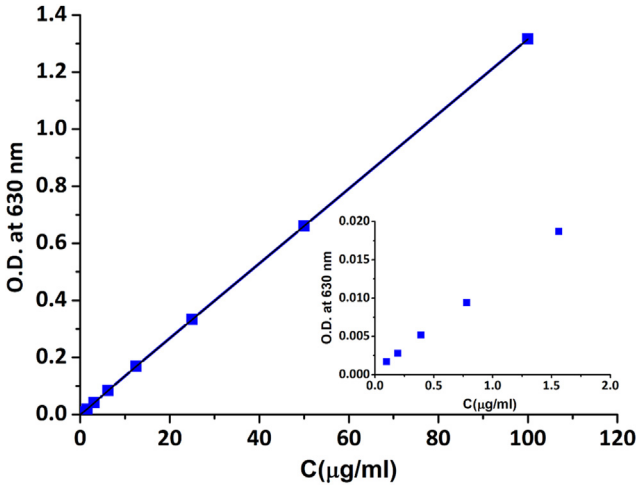

Figure 3. Spectrophotometry data obtained by measuring ODs in 2 ml of aqueous suspensions of CPs at concentrations of 0.098, 0.195, 0.391, 0.781, 1.5625, 3.125, 6.25, 12.5, 25.0, 50.0 and 100 μg/ml. A small plot represents the enlarged segment of the general plot to make visible the mean OD values with corresponding deviations for the concentrations of 0.098–1.5625 μg/ml. Measurements were performed in duplicate and the data are expressed as mean ± standard deviation.

having a size less than 100 nm. In this publication, we investigated the biological activity of carbon particles with a size of 1.0 ± 0.2 microns, obtained from a highly activated and highly porous carbon material with a powerful sorption potential. All this taken together and in the absence of cytotoxicity, systemic toxicity and genotoxicity, and in the presence of antioxidant and radioprotective abilities can be considered as a promising means of therapy of pathological states, including oncology, in the pathogenesis of which the endogenous intoxication and oxidative stress play the important role. The results of this study will be able to explain some of the observed positive effects of the modern methods of sorption therapy usage and outline the prospects for the development of a new therapeutic area, which we called "endocorporeal therapy", in which carbon particles will play a central role.

2. Materials and methods

2.1. Method of carbon particles preparation

Carbon particles were produced after grinding the fine fraction of the activated carbon adsorbent beads with the diameter of 0.1 mm $\leq$ d $\leq$ 0.25 mm and bulk density of 0.15 g/cc. Carbon beads were obtained as a result of copolymerization of 2-methyl-5-vinylpiridine with styrene divinylbenzene, carbonization at 400 °C in the nitrogen atmosphere in the rotary kiln, setting in nitrogen atmosphere at 800 °C, activation by the steam at 860 °C in the rotary kiln up to the bulk density of 0.22 g/cc and reactivation of fluidized beads by the steam up to bulk density of 0.15 g/cc. Thereafter, carbon beads were milled at the frequency of 20 Hz. 100 ml of activated carbon suspension with concentration of 100 μg/ml was prepared using 10% dimethyl sulfoxide (DSMO), stirred by the strong magnetic force and pulverized. The obtained suspension of carbon particles was further diluted to the required concentration.

To determine the dark cytotoxicity of CPs in the culture of human malignant lymphocytes MT-4, the concentration of activated CPs in the suspension was increased up to 500 μg/ml.

Table 2. Adsorptive capacity of highly activated carbon beads before and after milling.

Samples	Methylene blue (init. conc. 1.5 mg/ml)	Vitamin B_{12} (init.conc. 1.0 mg/ml)	Bilirubin (init. conc. 21.95 mg/dL)	HSA (init.conc. 24.47 g/L)
	Adsorption (mg/g)			
Initial Carbon beads, $\gamma = 0.15$ g/cm^3, $V_s = 2.0$ cm^3/g	723.18	306.32	20.82	2.25
Carbon powder after milling carbon beads $V_s = 2.0$ cm^3/g, $\gamma = 0.037$ g/cm^3, $V_s = 2.0$ cm^3/g	938.00	543.58	73.16	4.48

2.2. Methods of study of physical-chemical properties of carbon particles

2.2.1. Scanning electron microscopy (SEM) and energy dispersive X-ray analysis (EDX)

Morphology of activated carbon adsorbent beads was investigated by SEM method using the scanning electron microscope SEC miniSEM SNE 4500MB (SEC Co., Ltd, South Korea). Elemental analysis of the adsorbent beads was performed by EDX method using an EDAX Element PV6500/00 F analyzer. To perform SEM and EDX measurements, carbon adsorbent beads were deposited on the carbon tape.

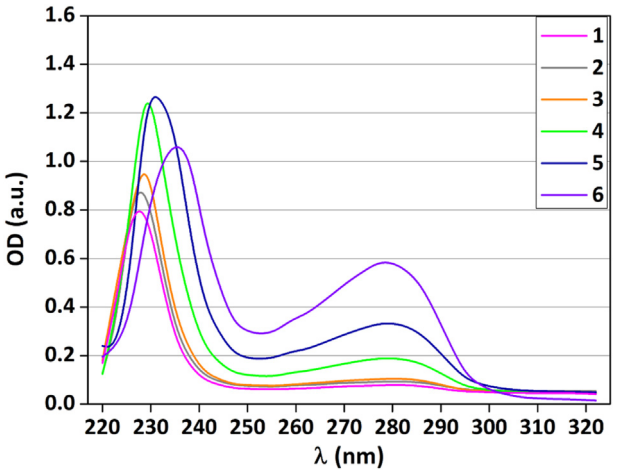

Figure 4. Spectrophotometry data obtained by measuring ODs of solution of BSA (0.05%) (1), aqueous suspensions of BSA (0.05%) and CPs at concentrations of 0.111 (2), 0.125 (3), 0.250 (4), 0.333 (5) and 0.500 (6) mg/ml. Measurements were performed in duplicate.

2.2.2. X-ray diffraction analysis (XRD)

The structure of obtained CPs was investigated by XRD analysis using diffractometer DRON-4 (CuKα-radiation). XRD patterns were processed using software package Origin Pro 9.0.

2.2.3. Transmission electron microscopy (TEM)

Morphology of activated carbon particles was investigated by TEM analysis. To perform the analysis, CPs were deposited on the copper grid coated by the formvar film. CPs were analyzed using microscope JEOL JEM-1230. Average sizes of CPs were calculated according to TEM data using software packages Image Tool 3 and Origin Pro 9.0.

2.2.4. Dynamic light scattering (DLS)]

Behavior of carbon particles in the suspensions was investigated by DLS method. CPs were dispersed in 0.9%-solution of sodium chloride by sonification for 5 min. The hydrodynamic diameter of activated CPs was measured using 1 ml of aliquot with concentration of carbon particles of 25 μg/ml by DLS method using Litesizer 500 (Anton Paar GmbH, Austria) equipped with the semiconductor laser diode (40mW, λ = 658nm) at 20 ± 1°C.

2.2.5. UV spectroscopy of the aqueous suspensions of carbon particles

The aqueous suspension of carbon particles of 100 μg/ml after sonication was serially diluted in a 2-fold manner making the range of concentrations ending at 0.2 μg/ml (the total volume of suspension in each dilution was at least 2 ml). The optical densities (ODs) of CPs suspensions were measured with a DU 70 Spectrophotometer (Beckman, USA) at 630 nm. The blank samples (pure water) were used to subtract their OD values from the OD values of carbon particles suspensions. The experiments were performed at 25 °C.

2.2.6. Adsorptive properties of carbon particles

Adsorptive capacities of carbon particles towards methylene blue (M.w. = 319.85 g/mol), vitamin B_{12} (M.w. = 1355.38 g/mol), bilirubin

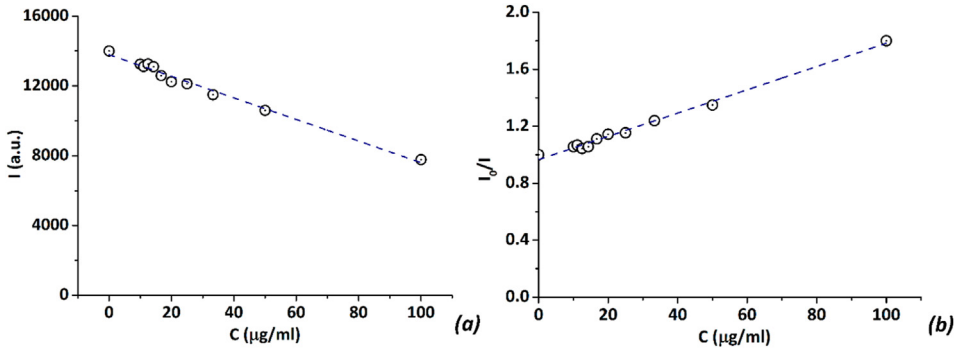

Figure 5. Intensities of intrinsic fluorescence of BSA (constant concentration 1.0 mg/ml, 1.5×10^{-5} M lit^{-1}) before and after interaction with different concentration of CPs. $\lambda_{ex} = 295$ nm, $\lambda_{em} = 340/40$ nm (a) and Stern-Volmer plot *vs* concentration of CPs (b).

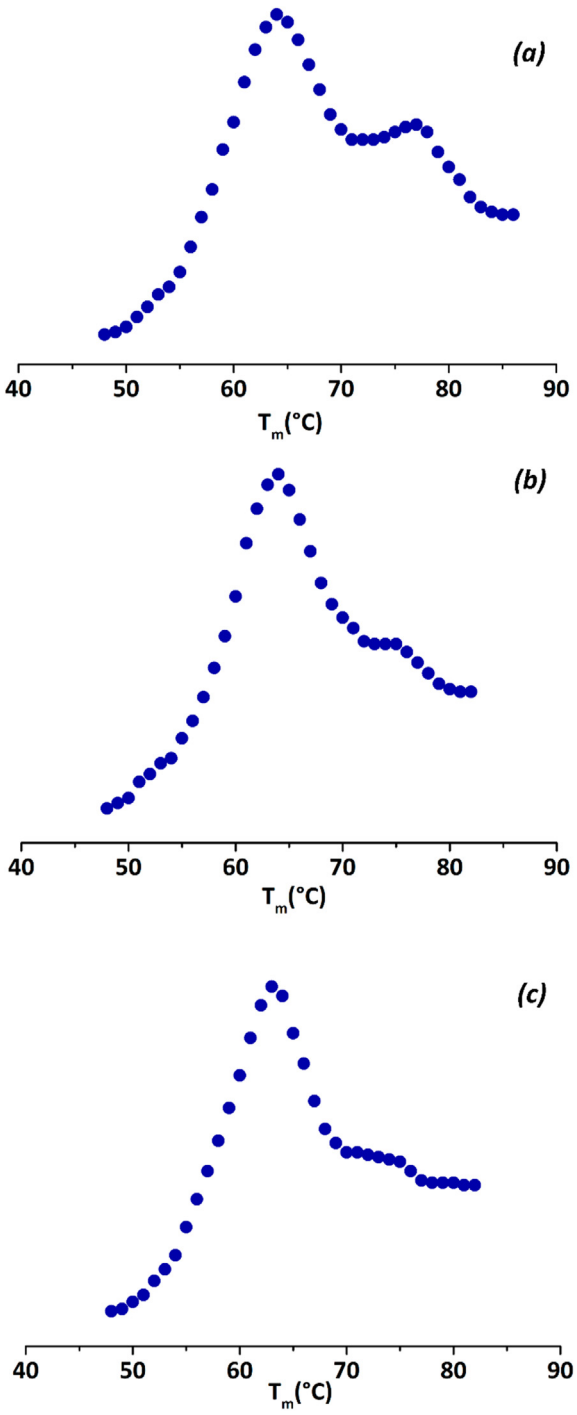

Figure 6. Melting thermogram of BSA before (a) and after the contact with carbon surface of CPs at the concentrations of 50 (b) and 100 μg/ml (c).

(M.w. = 584.66 g/mol) and human serum albumin (HSA) (M.w. = 67000 g/mol) were measured at the ambient temperature using orbital shaker (OS-20, BioSan) (rpm = 150). Two milliliters of testing solution poured into a glass-weighing beaker containing 2.15 ± 0.05 mg of carbon material. Contact time was 120 min. Concentrations of methylene blue and vitamin B_{12} were measured spectrophotometrically at λ = 630 and 360 nm respectively and calculated using the calibration graphs. Concentrations of bilirubin and HSA were determined using corresponding bilirubin or albumin Assay Kits (Sigma).

Table 3. *In vitro* effect of the carbon particles on 3T3-A31 mouse fibroblast cell line viability and proliferation.

% DMSO content	Number of living cells (% (M±m))	Carbon particles concentration (μg/ml; (% DMSO content))	Number of living cells (% (M±m))
5.0	20.0 ± 0.3	53.18; (5.0)	23.1 ± 0.4
2.5	**39.2 ± 0.1**	**26.6; (2.5)**	**41.7 ± 0.5**
1.25	**53.5 ± 0.2**	**13.3; (1.25)**	**57.3 ± 2.3**
0.62	73.8 ± 2.8	6.65; (0.62)	79.2 ± 1.7
0.31	97.0 ± 2.5	3.32; (0.31)	102.4 ± 1.4
0.16	100.2 ± 0.4	1.66; (0.16)	104.9 ± 1.7
0.08	98.8 ± 3.4	0.83; (0.08)	102.4 ± 1.2
0.04	98.7 ± 2.3	0.42; (0.04)	99.0 ± 1.3
0.02	99.4 ± 2.5	0.21; (0.02)	99.2 ± 1.1
0.01	100.7 ± 3.1	0.1; (0.01)	98.9 ± 1.4
IC_{50} values for the tested substance in 3T3-A31 mouse fibroblast cell line			
Substance name		IC_{50} value	
DMSO		**1.1 ± 0.2%**	
Carbon particles; (% DMSO content)		**17.98 μg/ml; (1.6 ± 0.3%)**	

2.3. Carbon particles interaction with BSA

2.3.1. UV spectroscopy of the interaction of carbon particles and BSA

The absorbance properties of BSA molecule after interaction with carbon particles at the different concentrations were investigated by the measurements on a NanoDrop ND3330 (NanoDrop,USA). The blank samples (pure water) were used to subtract their OD values from the OD values of CPs suspensions. The experiments were performed at 25 °C.

2.3.2. Fluorescence spectroscopy of the interaction of carbon particles and BSA

Steady state fluorescence was acquired on a Synergy HT multi-detection microplate reader (BioTek Instruments, Winooski, VT, USA). Intrinsic fluorescence of BSA (constant concentration 1.0 mg/ml) before and after interaction with different concentration of CPs was measured by the excitation at 296 nm and the emission at 340/30 nm. The experiments were performed on a BioTek Instruments Synergy HT Microplate Reader, (USA) at 25 °C.

2.3.3. Differential scanning microcalorimetry of the interaction of carbon particles and BSA

Melting thermograms of BSA before and after interaction with different concentration of CPs were recorded on DASM-4 microcalorimeter (Biopribor, Russia) at a scanning rate of 1 °C/min.

2.4. Study of carbon particles effect on the viability and proliferation of mammalian cells of different histogenesis

2.4.1. Cell culture

Studies were performed using *in vitro* models of mouse bone marrow cells (MBMC), mouse endothelial cells (MAEC cell line), bovine kidney cells (MDBK cell line), and mouse fibroblasts (3T3A31 cell line). Cell lines were obtained from the Bank of Cell Lines of Human and Animal Tissues of the RE Kavetsky Institute of Experimental Pathology, Oncology and Radiobiology of the NAS of Ukraine.

MAEC, MDBK and 3T3A31 cell lines were cultivated in the DMEM medium (Biowest, France) with 10% fetal bovine serum (FBS) (Biowest, France) and 40 μg/ml gentamycin (Sigma, USA). Mouse bone marrow cells were cultured in RPMI1640 medium (Biowest, France) with 10% FBS and 40 μg/ml gentamycin. Cells were cultivated in the cultural plastic laboratory glassware (SPL, Korea) in the humidified atmosphere

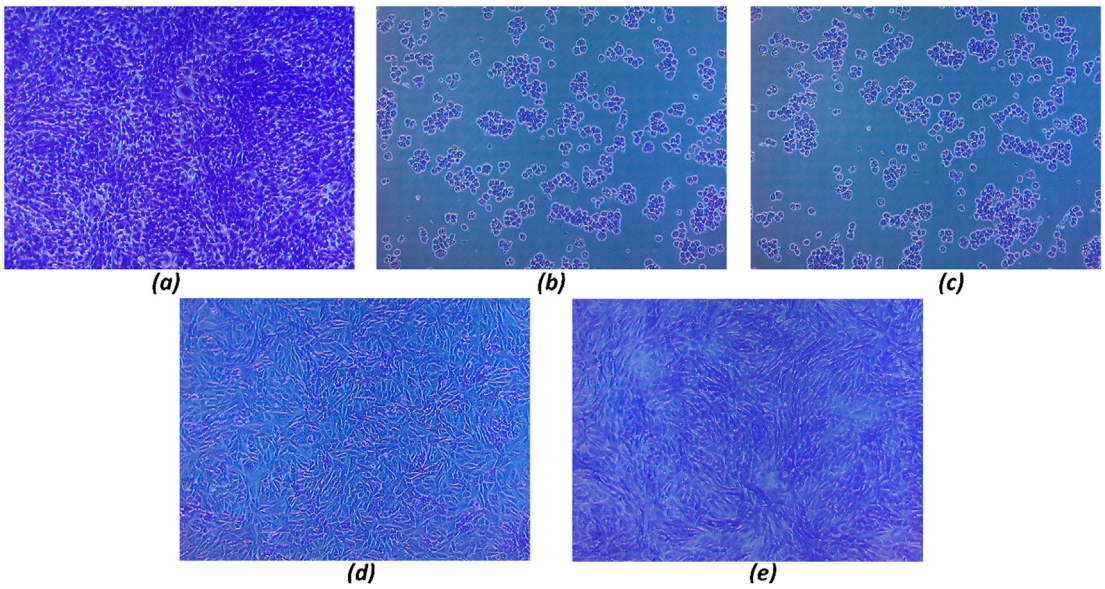

Figure 7. 3T3-A31 cells after the CPs treatment, crystal violet staining: a - control 3T3-A31; b - 3T3-A31 + DMSO (5.0 %); c - 3T3-A31 + CPs (2.6 μg/ml (5.0% DMSO)); d - 3T3-A31 + DMSO (1.25 %); e - 3T3-A31 + CPs (13.3 μg/ml (1.25 % DMSO)). For all figures magnification was ×100.

under 5% CO_2 and 37°C (CO_2-incubator, Heal Force, China). Medium exchange and cell culture passage were carried out using the standard method [19]. The cells passage was made in Versene solution (Vetline agroscience, Ukraine), after the cells achieved 70% monolayer. The exponentially growing cells were used in the experiments.

2.4.2. Cell viability measurement by the colorimetric method

To evaluate the effect of the carbon particles solution on the viability and proliferation of the cells, 24 hours after the last passage the test cells were seeded at a concentration of 1×10^4 cells/well in the wells of a 96-well plate (SPL, Korea) in DMEM/RPMI1640 medium with 10% FBS and 40 μg/ml gentamicin. Cells were cultivated during 24 hours in the humidified atmosphere under 5% CO_2 and 37 °C. Thereafter, the carbon particles in different concentrations, each 4 times repeated was introduced into the corresponding wells of the 96-well plates. Since the aqueous solution of carbon particles contains 10% dimethyl sulfoxide (DMSO), a 10% aqueous solution of DMSO (Applichem, Germany) was used as a positive control. Immediately after the introduction of the tested agents, the cells were placed into a CO_2 incubator and cultured for another 48 hours at 5% CO_2 and 37 °C. Upon completion of incubation with the agents, the viability and proliferative activity of the experimental cells were evaluated via colorimetric methods by staining the cells with crystal violet dye (Sigma, USA) [20].

The medium was removed and 50 μl of crystal violet solution (5 mg/ml dye in 70% methyl alcohol (Hotei, Netherlands)) was added to the each well. After 10 min, the dye was washed three times with running water. The plate was dried in the air under the room temperature in a dark place during 12 hours. The dye was extracted with 100 μl per well of 96% ethanol (Ukrmedspirt, Ukraine). The results were registered at 540 nm using a spectrophotometer (Labsystems Multiskan PLUS, Finland) with vertical beam. Number of the living cells (X) in the each well was evaluated in percent, calculating by the formula:

Table 4. *In vitro* effect of the CPs on MBMC viability and proliferation.

% DMSO content	Number of living cells (% (M±m))	Carbon particles concentration (μg/ml; (% DMSO content))	Number of living cells (% (M±m))
5.0	3.9 ± 3.3	53.18; (5.0)	2.7 ± 1.4
2.5	**41.5 ± 3.2**	**26.6; (2.5)**	**65.5 ± 4.4**
1.25	**73.5 ± 0.2**	**13.3; (1.25)**	**97.5 ± 3.3**
0.62	**88.1 ± 2.1**	**6.65; (0.62)**	**100.7 ± 2.6**
0.31	96.6 ± 1.7	3.32; (0.31)	99.7 ± 2.2
0.16	100.1 ± 1.6	1.66; (0.16)	101.0 ± 1.6
0.08	100.0 ± 2.1	0.83; (0.08)	101.6 ± 1.8
0.04	101.6 ± 4.9	0.42; (0.04)	101.6 ± 1.5
0.02	98.5 ± 0.3	0.21; (0.02)	101.6 ± 2.4
0.01	99.7 ± 2.9	0.1; (0.01)	99.4 ± 1.4
IC_{50} values for the tested substance in MBMC			
Substance name		IC_{50} value	
DMSO		**2.1 ± 0.1%***	
Carbon particles; (% DMSO content)		**31.5 μg/ml; (3.1 ± 0.2%)***	

* Note: the indices differ of one another significantly, $p\leq0.05$.

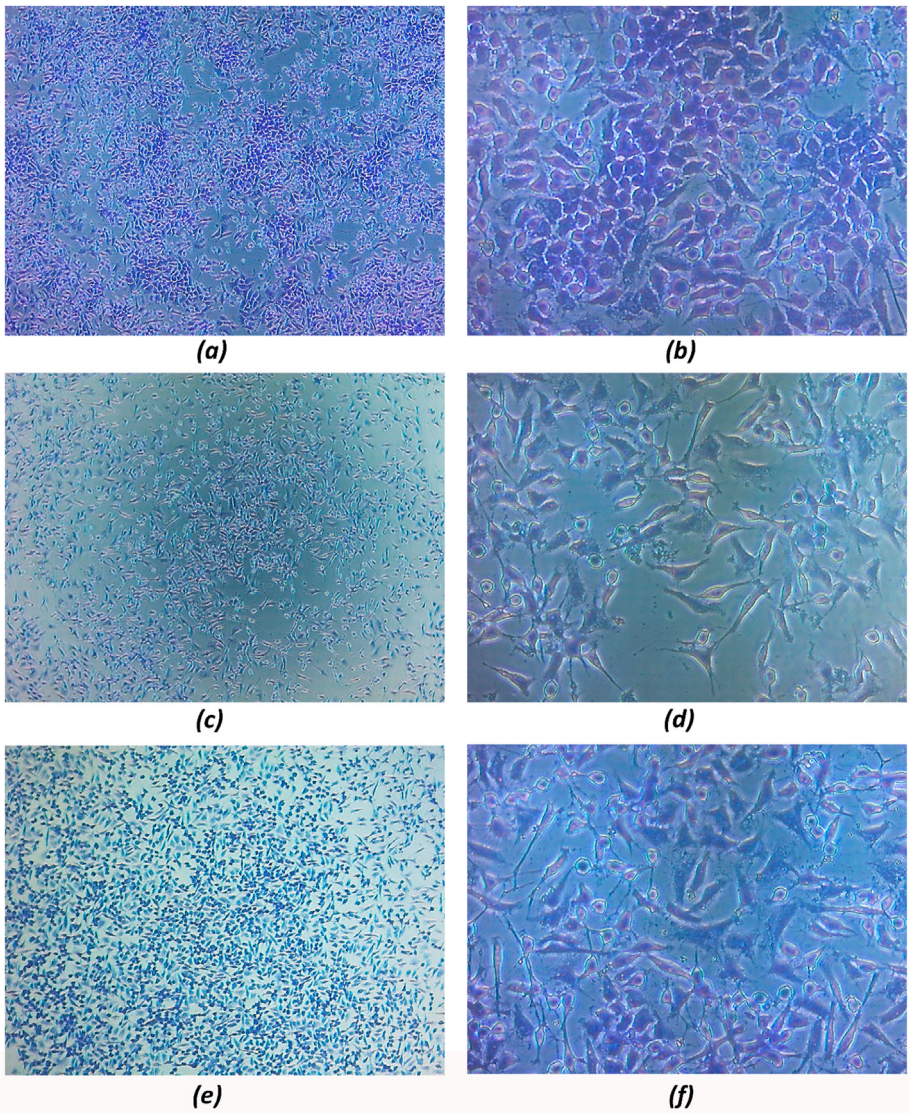

Figure 8. MBMC after the carbon particles treatment, crystal violet staining: a – control MBMC, magnification ×100; b - control MBMC, magnification ×400; c - MBMC + DMSO (2.5%), magnification ×100; d - MBMC + DMSO (2.5%), magnification ×400; e - MBMC + CPs (26.6 μg/ml (2.5%)), magnification ×100; f - MBMC + CPs (26.6 μg/ml (2.5%)), magnification ×400.

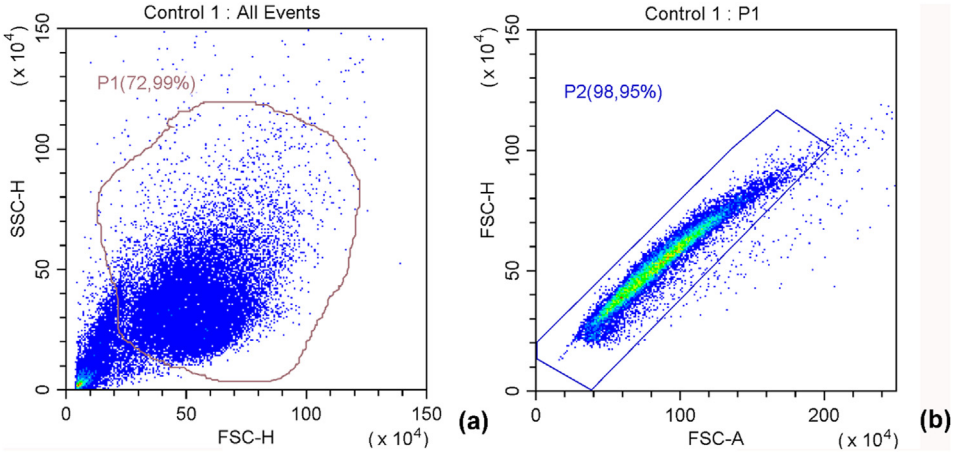

Figure 9. Gating strategy. Representative pseudo color plots illustrate cell population gating based on FSC-H and SSC-H parameters (a) and duplet discrimination using FSC-A and FSC-H parameters (b).

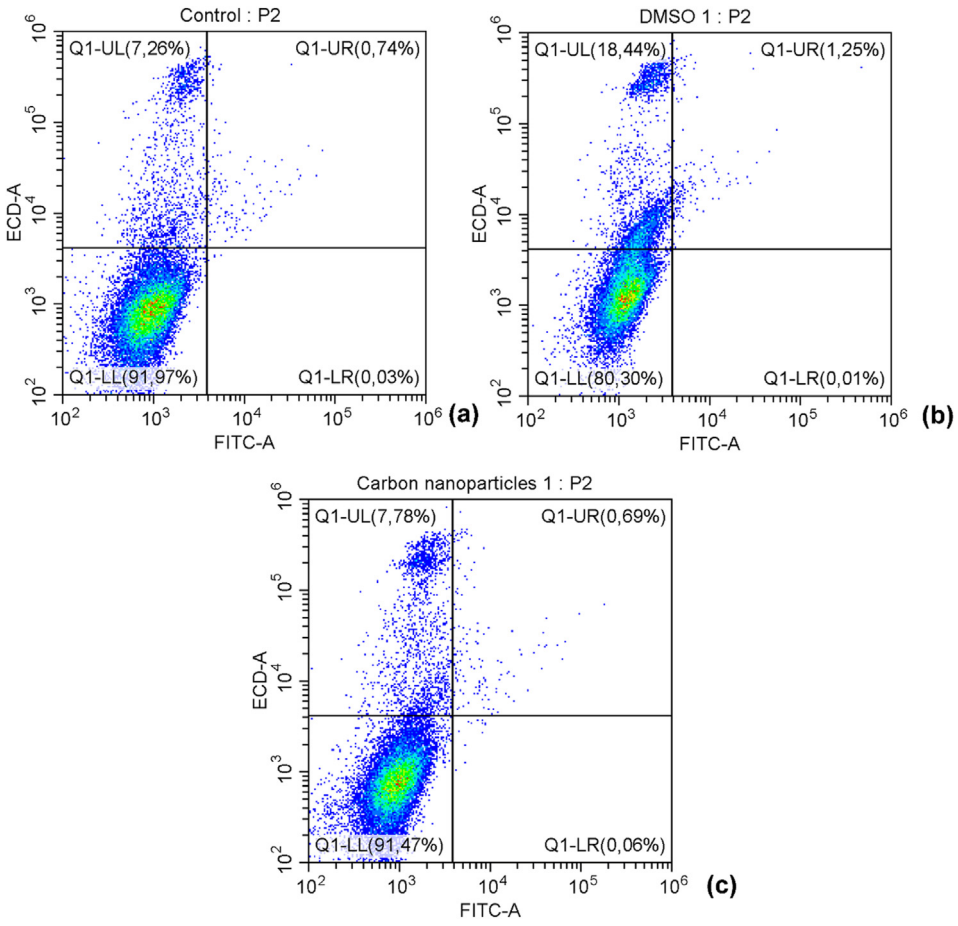

Figure 10. Representative dot-blots of the mouse bone marrow cells after DMSO or DMSO + carbon nanoparticles administration and farther staining with Annexin V/PI: (a) - control (intact cells); (b) - bone marrow cells + DMSO; (c) - bone marrow cells + DMSO + carbon nanoparticles.

Table 5. *In vitro* effect of the carbon particles and DMSO on MBMC death.

	Necrosis (%)		Early apoptosis (%)		Late apoptosis (%)	
	M	m	M	m	M	m
Control	7.37	0.80	0.04	0.01	0.78	0.03
DMSO	17.73*	0.63	0.03	0.01	1.64*	0.20
Carbon particles	8.06#	0.15	0.05	0.01	0.84#	0.08

Note. * - $p < 0.05$ versus control, # - $p < 0.05$ versus DMSO alone.

$$X = \frac{A_1 \cdot 100\%}{A_0},$$

where A_0 — an average optical density in the wells of control cells, A_1 — an average optical density in the experimental group well or positive control well. IC50 was calculated by the regression analysis method.

2.4.3. Statistical analysis

Average value (M) of the indices was measured and standard deviation of the average (m) was performed using Excel 2016 program package. Statistical processing of the obtained data was performed using the mathematical program for medical-biological statistics STATISTIS 6.0 using the Student's t-test; differences with a probability of at least 95% ($p < 0.05$) were considered significant.

2.5. Determination of dark cytotoxicity of carbon particles in the culture of human malignant lymphocytes MT-4

Cells of the MT-4 line were grown in a complete nutrient medium of RPMI-1640 (Sigma Aldrich, USA) with 2% L-glutamine, 10% embryonic calf serum (ETC, Biowest, France) and 40 μg/ml gentamicin at 37 °C and wet atmosphere with 5% CO_2. Replacement 1/2 of the medium was carried out every 2–3 days. For the experiment, cells at a concentration of 5×10^5 cells per milliliter of RPMI medium were co-cultured with carbon particles at the concentrations of 500, 250, 100, 50, 10, 5 μg/ml. After 24 hours of contact, vitality of the cells was determined using the trypan blue whistle color.

2.6. Determination of in vivo toxicity of carbon particles

The study was performed on female Wistar rats with the bodyweight between 190g ± 10g, obtained from the vivarium of the RE Kavetsky Institute of Experimental Pathology, Oncology and Radiobiology of the NAS of Ukraine. The animals were kept in accordance with the "Standard rules for the organization, equipment and maintenance of experimental biological clinics (vivariums)". When working with animals, all the requirements of the "European Convention for the Protection of Vertebrate Animals Used in Experimental and Other Scientific Purposes" (Strasbourg, 1986), the basic rules of good laboratory practice GLP (1981), the

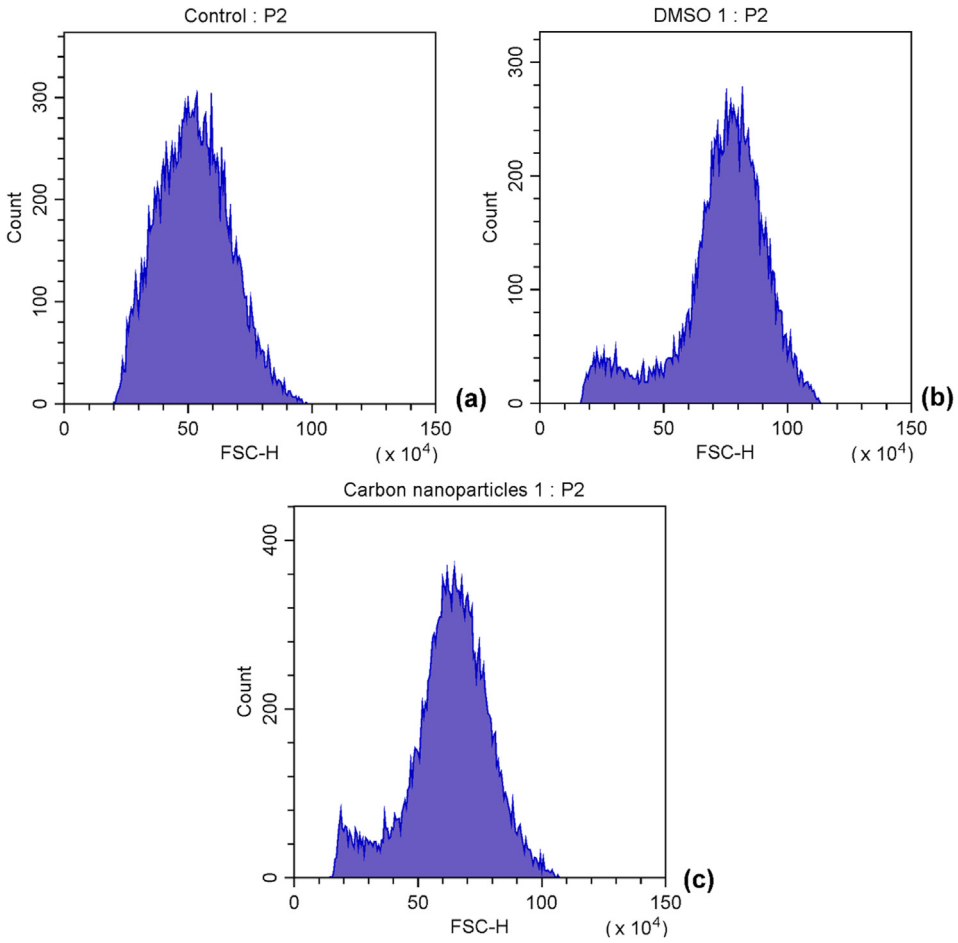

Figure 11. Representative histograms (distributions) of the mouse bone marrow cells according to their size after DMSO or DMSO + carbon nanoparticles administration: (a) - control (intact cells); (b) - bone marrow cells + DMSO; (c) - bone marrow cells + carbon nanoparticles.

law of Ukraine № 3447-IV of 21.02.2006 "On the protection of animals from cruel treatment" were held.

To investigate the *in vivo* toxicity of carbon particles, they were daily injected intraperitoneally (i.p.) to the rats for two weeks. The detailed experimental scheme is presented in Table 1. After finishing injection, rats were kept under observation for one month.

2.7. Determination of the genotoxicity of carbon particles

Assessment of the DNA damage level in the lymphocytes of the rats of group IV was performed using the cell gel electrophoresis (DNA Comet Assay) [21]. The suspension of lymphocytes ($1–2\times10^5$ cells/ml) was mixed with 1% low melting point (LMP) agarose (Sigma-Aldrich) at 37 °C, after which 75 μl of this mixture was distributed on agarose-pretreated with 1% agarose with normal melting point (Sigma-Aldrich). Three slides were grown for each sample. After agarose cooling, the slides were immersed into a cooled lysis solution (2.5 M NaCl, 100 mM EDTA, 10 mM Tris base, 10% DMSO, 1% Triton X-100, pH 10) and kept for 12 hours at 4 °C. After lysis, the slides were placed into the electrophoresis canister for horizontal electrophoresis and incubated in an alkaline buffer (300 mM NaOH, 1 mM EDTA, pH > 13) for 20 min. Electrophoresis was performed in the same solution at a voltage of 0.8 V/cm for 20 min. Afterwards, the slides were washed in the neutralization solution (0.4 M Tris–HCl, pH 7.5) for 10 min and then twice washed in the distilled water for 5 min. Then the slides were dried at 37 °C and stained with SYBR Green I solution. The analysis of the preparations was performed on an Axio Scope A1 fluorescence microscope. The obtained digital images of DNA comets were analyzed using CometScore software (TriTek Corp., USA). At least 50 randomly selected comets from each test sample were analyzed. The level of DNA damage was assessed by the percentage of DNA in the comet's tail (% tail DNA) and tail moment (TM).

Statistical analysis was performed using the GraphPad Prism 6 software package. The mean value and standard deviation of the mean (SD) were determined in the analysis of the results. The Mann-Whitney U-test was used to assess differences between groups. The degree of significance was taken at the level of $p < 0.05$.

2.8. Determination of the number of dead and live cells in a population by the method of evaluating the level of membrane phospholipid inversion

Mouse bone marrow cells were cultivated in the RPMI 1640 medium with 10% CFS and 40 μg/ml Gentamycin, in the cultural plastic laboratory glassware in the humidified atmosphere under 5% CO_2 and 37°C. Medium exchange and cell culture passage were carried out using the standard method. The exponentially growing cells were used in the experiments.

Mouse bone marrow cells were sowed into the wells of a 12-well plate ($0.12x10^6$/well in the RPMI 1640 medium with 10% CFS and 40 μg/ml Gentamycin. The cells were cultivated in the humidified atmosphere under 5% CO_2 and 37°C during 24 hours. Then, the carbon particles (up to 11.7 μg/ml end concentration) or DMSO (up to 1.1% end concentration) were added into the corresponding wells. After this, the cells were cultivated during the next 48 hours in the humidified atmosphere under 5% CO_2 and 37 °C.

After 48-hour incubation, the mouse bone marrow cells were washed off the substrate with trypsin-EDTA and washed clean with phosphate-

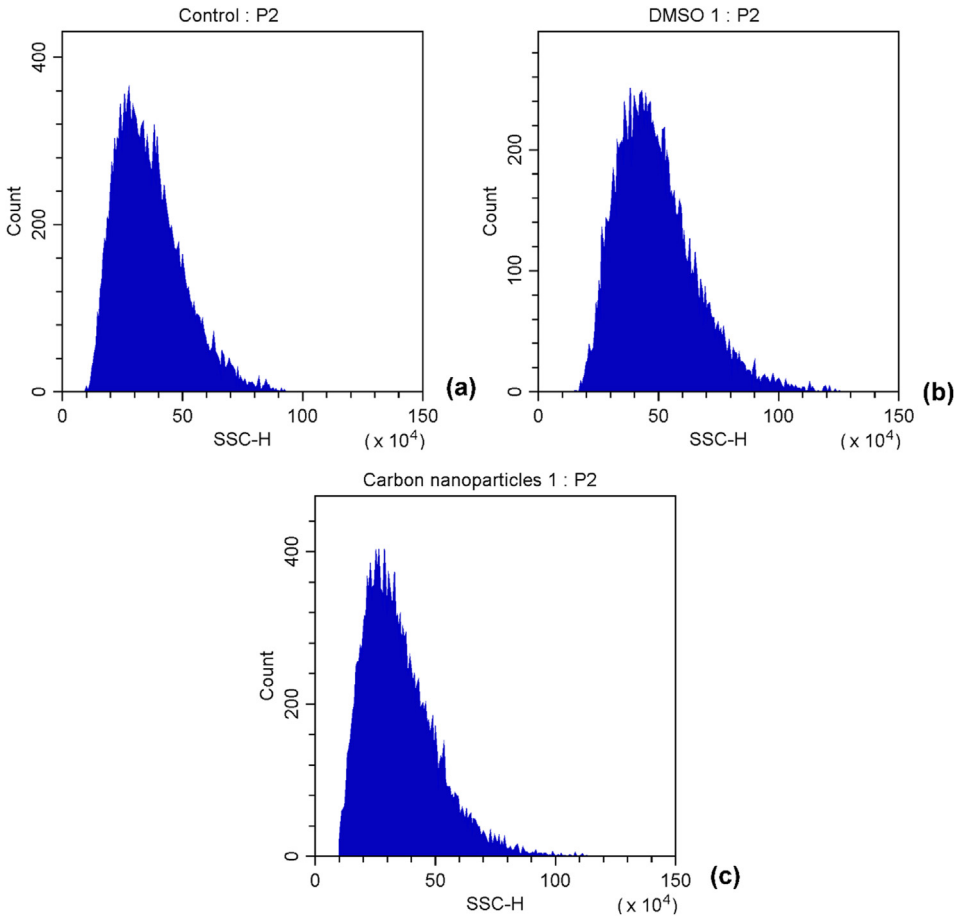

Figure 12. Representative histograms (distributions) of the mouse bone marrow cells distribution according to their intracellular grain after DMSO or DMSO + carbon nanoparticles administration: (a) - control (intact cells); (b) - bone marrow cells + DMSO; (c) - bone marrow cells + carbon nanoparticles.

saline buffer. To stain the cells with Annexin V/PI, the Dojindo (Japan) kit was used. Staining was performed accordingly to the manufacturer's protocol under the room temperature. Immediately after staining, the cells were analyzed in the DxFLEX flow cytofluorimeter, Beckman Coulter. Gating with FSC-H/SSC-H dot-plot was carried out to select the necessary cell population and discrimination of the duplets on FSC-A/FSC-H dot-plot was made. The alive/dead ratio was analyzed on the dot-blot with quadrants in FITC-A/ECD-A co-ordinates. Each influence was repeated in three parallels.

3. Results

3.1. Characterization of the carbon particles

Microstructure of the initial activated carbon adsorbent beads was investigated via SEM method; representative SEM-image is shown in Figure 1a. An average diameter of the carbon beads calculated according to the obtained data equals 0.47–0.65 μm. Results of elemental analysis (EDX) indicate that these beads contain pure carbon without any additional impurities.

Structure of the carbon particles was investigated via XRD method; corresponding pattern is presented in Figure 1b. As it can be observed, there are two wide peaks centered at $2\theta = 21.1^\circ$ and 43.5° in the pattern of the investigated sample. These peaks correspond to the atomic planes (002) and (100) respectively of the graphite structure [22]. The shape of the peaks – wide with the absence of the clear maximum – points on the mostly amorphous structure of the investigated carbon particles. However, two clear signals can be seen at $2\theta = 21.5^\circ$ and 23.9°, which indicate on the beginning the crystallization of the carbon particles and appearance of small microcrystalline inclusions with the graphite structure.

XRD data of the synthesized carbon particles are in good agreement with the TEM investigations of the particle's morphology. Representative TEM images of carbon are shown in Figures 2a and 2b. As it is seen, CPs are mostly amorphous (Figure 2a), but some crystalline NPs with the average sizes of 100–110 nm are present in the investigated sample (Figure 2b).

Obtained carbon particles were dispersed in 0.9%-solution of NaCl in presence of 10% of DMSO. The behavior of the CPs in such suspension was investigated via DLS method. According to the obtained results, the hydrodynamic diameter of carbon particles was 1125.3 nm (Figure 2c). Polydispersity index of CPs in the suspension equals 0.092, which indicates that such particles are highly monodispersed.

The spectrophotometry of the aqueous suspensions of CPs diluted within the wide range of concentrations (0.098–100.0 μg/ml) was carried out (Figure 3). In order to clarify whether this particular range of concentrations of CPs can be completely determined by the spectrophotometry, which is important for calibration purposes, the optical densities (ODs) were recorded at 630 nm as described earlier [23]. Figure 3 demonstrates the strictly linear dependence between concentrations of CPs and corresponding ODs with the capability to detect these particles diluted as low as 0.098 μg/ml.

As a result of grinding, the adsorption potential of the milling fine fraction of carbon beads increases significantly (Table 2).

From Table 2, one can see that nanosized carbon particles possess much higher adsorptive activity than initial granular carbon adsorbent measured towards methylene blue dye, vitamin B_{12}, bilirubin and human serum albumin.

Table 6. *In vitro* effect of the carbon particles on MDBK cells viability and proliferation.

% DMSO content	Number of living cells, (% (M±m))	Carbon particles concentration (μg/ml; (% DMSO content))	Number of living cells (% (M±m))
5.0	1.6 ± 0.1	53.18 (5.0)	1.7 ± 0.2
2.5	**25.1 ± 0.3**	**26.6 (2.5)**	**22.6 ± 1.3**
1.25	**56.3 ± 0.8**	**13.3 (1.25)**	**59.0 ± 2.3**
0.62	76.8 ± 0.5	6.65 (0.62)	80.3 ± 2.0
0.31	86.3 ± 1.2	3.32 (0.31)	92.8 ± 1.3
0.16	93.6 ± 2.7	1.66 (0.16)	93.6 ± 1.0
0.08	99.8 ± 0.9	0.83 (0.08)	101.3 ± 1.1
0.04	100.7 ± 4.2	0.42 (0.04)	100.8 ± 1.3
0.02	102.9 ± 1.6	0.21 (0.02)	101.1 ± 1.0
0.01	102.2 ± 1.7	0.1 (0.01)	100.6 ± 1.1
IC_{50} values for the tested substance in MDBK bovine kidney cell line			
Substance name		IC_{50} value	
DMSO		**1.4 ± 0.1%**	
Carbon particles; (% DMSO content)		**18.1 μg/ml; (1.3 ± 0.1%)**	

Table 7. *In vitro* effect of the carbon particles on MAEC mouse endothelium cell line viability and proliferation.

% DMSO content	Number of living cells (% (M±m))	Carbon particles concentration (μg/ml; (% DMSO content))	Number of living cells (% (M±m))
5.0	23.8 ± 0.3	53.18 (5.0)	17.8 ± 0.2
2.5	**42.5 ± 1.0**	**26.6 (2.5)**	**43.4 ± 0.6**
1.25	**65.8 ± 0.3**	**13.3 (1.25)**	**66.7 ± 0.7**
0.62	82.4 ± 2.7	6.65 (0.62)	82.6 ± 2.9
0.31	88.2 ± 0.4	3.32 (0.31)	91.1 ± 1.3
0.16	97.5 ± 3.0	1.66 (0.16)	99.1 ± 1.0
0.08	98.8 ± 2.7	0.83 (0.08)	101.1 ± 1.4
0.04	100.2 ± 2.5	0.42 (0.04)	101.2 ± 1.8
0.02	101.6 ± 3.9	0.21 (0.02)	101.2 ± 1.1
0.01	100.8 ± 3.7	0.1 (0.01)	99.8 ± 1.3
IC_{50} values for the tested substance in MAEC mouse endothelium cell line			
Substance name		IC_{50} value	
DMSO		**1.4 ± 0.1%**	
Carbon particles; (% DMSO content)		**43.9 μg/ml; (1.7 ± 0.1%)**	

The interaction of BSA and CPs was registered by UV- spectroscopy method in the far-ultraviolet region.

The observed absorbance spectral changes of BSA loaded with CPs (Figure 4) in the near-ultraviolet range indicate on the appearance of conformational perturbations caused by CPs interaction with BSA, leading to slight opening the molecular domain structure. Two tryptophan residues and some of tyrosine residues, which initially were exposed to some internal hydrophobic surfaces, became accessible to the solvent molecules of light source. No red or blue shift was observed for BSA during its loading by carbon particles and suggested the absence of dissociation process.

The effect of CPs on fluorescence intensity of BSA is illustrated in Figure 5(a). The application of fluorescence spectroscopy usually uses to study the structure and conformation of plasma proteins. The emission characteristics of aromatic amino acids residues such as tryptophan, tyrosine, and phenylalanine in protein can provide a convenient tool for investigation of binding and conformation changes upon interaction with NPs [24]. The efficiency of this fluorescence quenching is dependent on the proximity of quencher and chromophore. Measurements of fluorescence quenching of proteins would reveal the information on the relative accessibility of carbon particles to protein chromophore group [25].

In presence of CPs, the intrinsic fluorescence spectra of BSA were quenched, which might arise from the change in the protein conformation probably due to the protein interaction with the surface of carbon particles, reflecting the relative changes in the proximity between Trp (active fluorescence emitter) in the protein and CPs (the quenching agent). The relative kinetic efficiency of BSA fluorescence quenching was estimated by fitting the dependence of I_0/I on carbon particles concentration (C) (Figure 5b). The plot of I_0/I versus concentration of CPs was linear that indicates on the occurrence of only one type of quenching. In such case, the dependence of fluorescence on the quencher concentration follows Eq. (1) [26]:

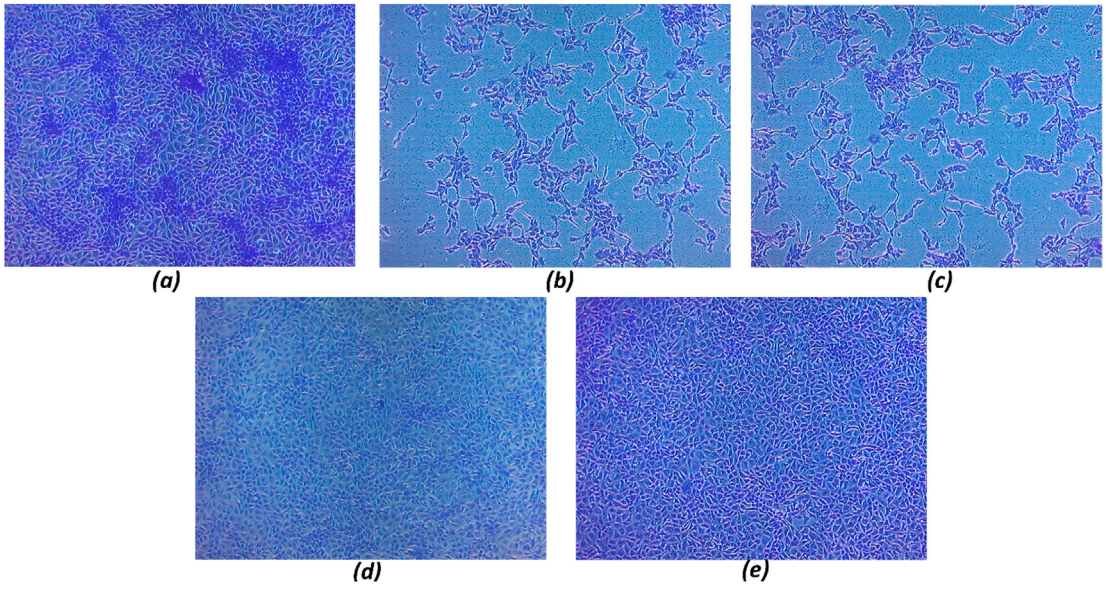

Figure 13. MDBK cells after the carbon particles treatment, crystal violet staining: a - control MDBK; b - MDBK + DMSO (2.5%); c - MDBK + CPs (26.6 μg/ml (2.5%)); d - MDBK + DMSO (1.25%); e - MDBK + CPs (13.3 μg/ml (1.25%)). For all figures magnification was ×100.

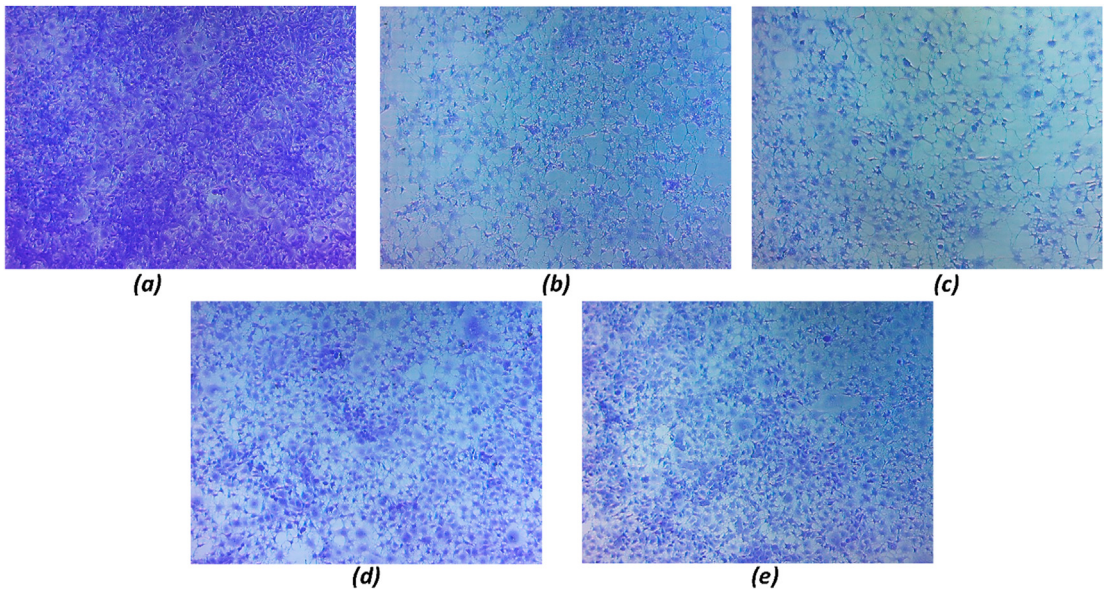

Figure 14. MAEC cells after the CPs treatment, crystal violet staining: a - control MAEC; b - MAEC + DMSO (5.0%); c - MAEC + CPs (53.18 μg/ml (5.0%)); d - MAEC + DMSO (2.5%); e - MAEC + CMNPs (26.6 μg/ml (2.5%)). For all figures, magnification was ×100.

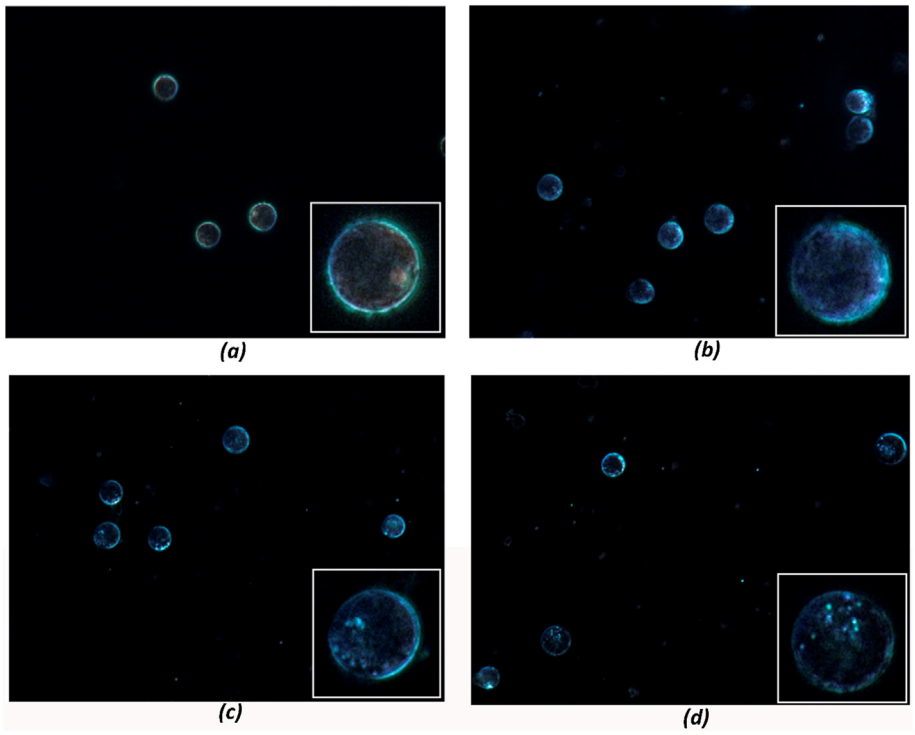

Figure 15. Accumulation of carbon particles on the surface of human malignant lymphocytes MT-4 cells after their 24-hour co-incubation: a - control, b - 100 μg/ml, c - 250 μg/ml, d - 500 μg/ml.

$$I_0/I = 1 + K_{sv}[C] = 1 + K_q r_0[C] \quad (1)$$

where I_0 and I denote fluorescence intensities of protein in the absence and presence of CPs respectively and K_{sv} is the Stern-Volmer quenching constant of BSA with CPs value derived from this plot is 9.6×10^1 lit.mol^{-1}. In Eq. (1) r_0 represents the lifetime of biopolymer fluorescence and has a value of 10^{-8} s [27] and calculated K_q showed the value of 9.6 $\times 10^9$, which points on the dynamic mechanism of complex formation between BSA and quencher, when the quencher and fluorophore come into contact during the life time of the excited state. The constant of association (K_{ass}) between BSA and CPs calculated on the base of data of Figure 5a is 0.33×10^3 M^{-1}, which indicates on the low affinity between protein and carbon surface. This is confirmed by the data obtained via DSC method, which indirectly indicates that after the contact with CPs, albumin does not change its thermal stability and can hold carbon

Table 8. Dark cytotoxicity of the carbon particles determined on human malignant lymphocytes MT-4 cell line.

Concentration C (μg/ml)	0	5	10	50	100	250	500
Cell death (%)	7.5	8	6.5	5.5	11	12,5	17
	8.5	6	8	7.5	8.5	8	24.5
	6.5	5.5	7	8	9.5	9	25
Average value	7.50	6.50	7.17	7.00	9.67	9.83	22.17
Standard deviation	1.00	1.32	0.76	1.32	1.26	2.36	4.48
Living cells (%)	92.50	93.50	92.83	93.00	90.33	90.17	77.83

particles due to the multiple hydrogen, electrostatic, hydrophobic etc. bonds. DSC method demonstrates the invariability of the bimodal shape of the melting thermograms and the position of the main maxima on them ($T_m = 64.0 \pm 0.01$ °C) before (a) and after the interaction of BSA with CPs (b, c) (Figure 6). The comparative analysis of these thermograms demonstrates only the gradual decrease of the amplitude and melting temperature of the second maximum of BSA from $T_m = 77.0$ °C (a) up to 75.6 and 74.7 °C (b, c) dependently on the concentration of CPs in the analyzed suspensions.

3.2. Effect of carbon particles on the viability of mammalian cells of various histogenesis

The estimation of the effect of carbon particles in different concentrations on the viability and proliferation of normal mammalian cells using a panel of cell lines of different histogenesis were carried out. These lines represent the tissue types, which are the most sensitive to the toxic substances, especially bone marrow and kidneys, or such tissues and cells as are present in all organs and systems (fibroblasts, endothelium). Moreover, these cell lines are of different species origin (mouse, bovine).

Based on Table 3 data, the IC_{50} values for the substance tested in the mouse fibroblast model were calculated by the regression analysis method. IC_{50} (the concentration of half-maximum inhibition) — the index of the drug concentration being necessary for 50% inhibition of the reaction tested *in vitro*. The results described above demonstrate that cytotoxic/cytostatic activity of the CPs were observed after the fibroblast culture treatment with the substance tested in 6.65–53.18 μg/ml, is caused not by CPs action but by DMSO toxicity (Table 3).

It was not any statistically significant difference between IC_{50} indices for DMSO and CPs (by the DMSO percentage): 1.1 ± 0.2% *vs* 1.6 ± 0.3% (Table 3, Figure 7). Therefore, the obtained data allow suggesting that the carbon particles as to themselves in their tested concentrations do not have cytotoxic/cytostatic activity as to 3T3-A31 mouse fibroblast cell line.

The *in vitro* investigations of CPs impact on the MBMC viability demonstrated that high cytotoxicity of the tested substances was caused by the high DMSO percentage in the test-sample solution (Table 4). The

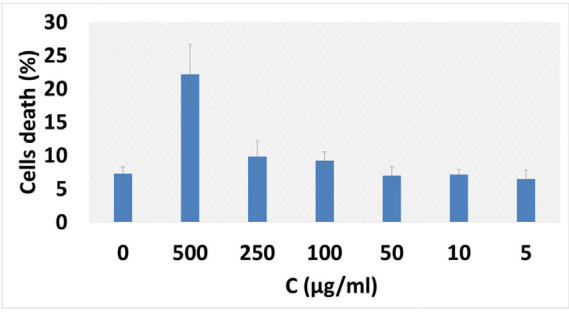

Figure 16. Dark cytotoxicity of the carbon particles determined on the human malignant lymphocytes MT-4 cell line.

Table 9. Results of in vivo toxicity of carbon particles investigation.

Group	Dose (mg/kg)	Number of animals	Mortality	LD_{50}	Cumulative dose (mg/kg)
I	0.2	5	0	Unobserved	2.8
II	0.4	5	0	Unobserved	5.6
III	1.6	5	0	Unobserved	22.4
IV	2.56	5	0	Unobserved	35.8

living cells amount was changed similarly in both experimental groups (Table 4).

At the same time, MBMC viability after their cultivation with CPs in different concentration or DMSO showed the significantly higher IC_{50} index for DMSO (2.1 ± 0.1% *vs* 3.1 ± 0.2%) in the colorimetric analysis. Thus, the obtained data allow suggesting that CPs do not have their own toxic impact on the MBM cells but even can inhibit the DMSO cytotoxic/cytostatic activity for these cells (Table 4, Figure 8).

The cell survival indices could be counted using FITC-A/ECD-A dot-plot. The dot-plots of the control MBMC, MBMC + DMSO or MBMC + DMSO + CPs demonstrated the percentage of the necrotic, early-apoptotic and late-apoptotic cells (Figure 9 and Figure 10). It was found that DMSO induces 2.4-fold necrotic cell death ($p<0.05$) versus control. Protective effect of CPs was revealed in their ability to abolish the necrosis induction, 2.2-fold diminishing the percentage of the necrotic MBMC ($p<0.05$) (Table 5). In such case, despite the fact that the percentage of the apoptotic MBMC was comparatively low, the difference was revealed.

DMSO alone 2.1-fold magnified percentage of the late-apoptotic MBMC ($p<0.05$), and the CPs 1.95-fold diminished this index ($p<0.05$) returning it to near-control value. Besides that, DMSO significantly modified such physical characteristics of MBMC as their size and granularity. The representative histograms of the FSC-H index reflecting cell size (Figure 11) demonstrated that after 48 hours of contact of MBMC with DMSO, the cell size distribution became bimodal compared to the unimodal distribution in the control cells, and the average cell size also increased significantly. CPs contributed to a decrease in MBMC size, but the distribution remained bimodal. Finally, histograms of the cell distribution according to their granularity, indicated with side scatter – SSC-H, demonstrated that DMSO significantly increased cell granularity – probably, in connection with cell vacuolization or enhanced lysosome amount. At the same time, the carbon particles have returned this index to the control level (Figure 12).

The viability analysis of the MDBK cells (bovine kidney cell line) after CPs or DMSO treatment demonstrate that the cytotoxic effect of the test solutions was caused not by CPs but by DMSO included into the solvent (Table 6, Figure 13). This conclusion was confirmed also by the IC_{50} indices for the tested substances– any significant difference was not found between them: 1.4 ± 0.1% – DMSO and 1.3 ± 0.1% - CPs.

The obtained data show that the MDBK cell line cultivation in presence of the carbon particles does not have any significant effect on the cells viability and proliferation (Table 6).

The viability analysis of the mouse endothelium cells (MAEC cell line) after CPs or DMSO treatment demonstrate that the cytotoxic effect of the test solutions was caused not by CPs but by DMSO included into the solvent (Table 7). As one may conclude, CPs in the concentrations of ≥3.3 μg/ml do not cause any toxic impact on the MAEC cells.

Table 10. The level of DNA damage in rat lymphocytes determined by comet phoresis

Group of animals	% tail DNA Mean ± SD	TM Mean ± SD
Intact rats (n = 5)	1.0 ± 0.2	0.03 ± 0.01
IV (n = 5)	1.3 ± 0.3	0.17 ± 0.06

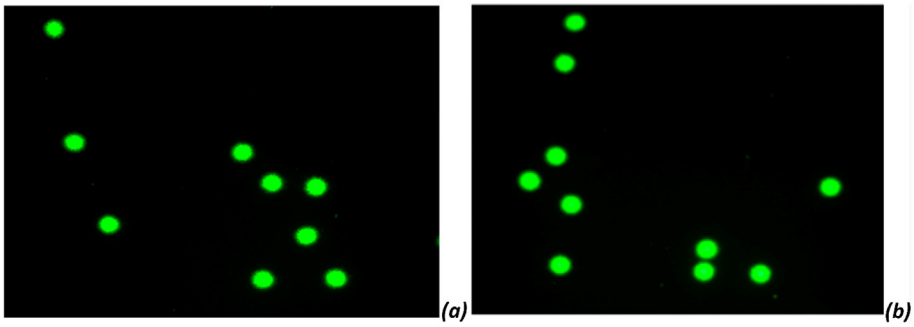

Figure 17. Representative images of DNA comets obtained from rat lymphocytes belonging to the group of intact tats (a), experimental IV group (b).

This conclusion was confirmed also by the IC_{50} indices for the tested substances – any significant difference was not found between them. Thus, the obtained data show that the CPs treatment of the MAEC cells does not have any significant negative effect on the cells viability and proliferation (Figure 14).

The results of the visual analysis show that carbon particles do not accumulate neither in the cytoplasm nor on the membrane surface of the normal cell lines of different histogenesis. The dark cytotoxicity method illustrated that in the case of MT-4 cell line (Figure 15), CPs adhere on the spherical surface of malignant lymphocytes in the form of luminous particles, which are clearly visible at a concentration of 250–500 μg/ml, and only at the highest concentration (500 μg/ml) exhibit cytotoxic effect on MT-4 cell line.

Determination of dark cytotoxicity of CPs towards the culture of human malignant lymphocytes MT-4 is summarized in Table 8 and Figure 16.

A one-month observation of the experimental animals showed the absence of mortality and any side effects after the intraperitoneal injection of CPs. LD_{50} in all groups was unobserved (Table 9).

In the group IV, the level of DNA damage in rat lymphocytes was assessed by the comet phoresis (Table 10, Figure 17). It was established that carbon particles injection does not induce DNA-damaging effect on lymphocytes of peripheral blood of experimental animals.

4. Discussion

This work describes a two-stage process for obtaining activated carbon particles with a high sorption potential for substances of different chemical nature. At the first stage, after obtaining a fraction of a granular carbon sorbent with a granule diameter of 0.47–0.65 mm and a bulk density of 0.22 g/cc, its additional activation was performed, and, as a result, the bulk density decreased up to 0.15 g/cc due to an increase in porosity, and sorption capacity significantly increased. The study of its microstructure (Figure 1a) showed that granules were pure carbon without any inclusions.

At the second stage, a fine fraction of sorbent granules with a diameter of 0.1 mm $\leq d \leq$ 0.25 mm obtained by sieving, were subjected to grinding at a frequency of 20 Hz. As a result of grinding, the finely dispersed carbon powder with high adsorption characteristics towards to marker substances, methylene blue dye, vitamin B_{12} and serum albumin, represents, respectively, a class of marker substances of low, medium and high molecular weight, as well as unconjugated bilirubin, which is a striking representative of protein-bound metabolites and toxins of a hydrophobic nature (Table 2), was obtained. Two signals recorded by the XRD method indicate on the beginning of the crystallization of carbon particles and the appearance of microcrystalline inclusions with a graphite structure (Figure 1b). TEM data confirmed that the carbon particles in the suspension were mostly amorphous, but they were also presented in the form of crystals of 100–110 nm in size (Figure 2b).

To prepare a suspension of CPs based on a saline solution, 10% dimethyl sulfoxide was used, which ensures its stability for 3 days. The hydrodynamic diameter of these particles in the suspension with a concentration of 100 μg/ml was 1125 nm, and the polydispersity index was 0.092, which indicates on their high monodispersity (Figure 2c). The concentration of these particles was monitored by spectrophotometry at a wavelength of 630 nm, which allowed very accurate detection of very low concentrations of CPs in the suspension (Figure 3).

Before the injection of carbon particles suspension to the experimental animals, the study of the mechanism of their interaction with the main protein of blood plasma – albumin – was carried out. To investigate the interaction of carbon particles with albumin, the methods of spectrophotometry and spectrofluorimetry are often used, which help to recorder the conformational shifts of the protein molecule that occur upon its contact with testing object.

A very high absorbance peaking near 187 nm predominantly belongs to peptide bonds, but it is strongly affected by traces of turbidity or the presence of carboxyl ions. In the near-ultraviolet range (240–400 nm), the absorbance spectra of albumin peaking near 280 nm are owed to the tryptophan and at 287 nm – to tyrosine residues, the difference in absorption readings offers predictions on the relative intramolecular location of tryptophan and tyrosine residues, and the occurrence of conformational perturbations is caused by CPs interaction with BSA (Figure 4).

Fluorescence, the immediate emission of light on radiation with monochromatic light, is largely attributed to the tryptophans of albumin, and only a small proportion belongs to the more numerous tyrosines, and depends on the wavelength of the exciting light. In the wavelength region between 295 and 305 nm, tyrosine residues are not excited, and only a pure tryptophans emission spectrum centered near 345 nm is seen. Contribution of tyrosines can be determined with excitation below 295 nm. Most experiments are concerned with tryptophan fluorescence and used excitation at $\geq$ 296 nm.

The effect of carbon particles on the fluorescence intensity of BSA is illustrated in Figure 5. In presence of nanoparticles, the intrinsic fluorescence of BSA was quenched (Figure 5a), which might arise from the change in the protein conformation, probably, due to the protein interaction with the surface of CPs, reflecting the relative changes in the proximity between Trp (active fluorescence emitter) in the protein and CPs (the quenching agent). To analyze the quenching mechanism, the relative kinetic efficiency of BSA fluorescence quenching was estimated. The linear plot of I_0/I versus concentration of CPs (Figure 5b) indicates on the occurrence of only one type of quenching [26] with the quenching constant 9.6×10^9 lit.$M^{-1}s^{-1}$, which points on the dynamic mechanism of complexing BSA with CPs. Additionally, calculated constant of association between protein and carbon ($K_{ass} = 0.33 \times 10^3$ M^{-1}) indicates on a low binding affinity between BSA molecules and CPs. Low affinity was confirmed by the data of differential scanning calorimetry, which demonstrated the invariability of the bimodal shape of the melting thermograms and the position at 64.0 ± 0.01 °C of the main maxima on them. The gradual decrease of the amplitude and melting temperature of

the second maximum of BSA from $T_m = 77.0$ °C for initial BSA up to 74.7 °C for BSA after the contact with CPs at a concentration of 100 μg/ml indicate that during their interaction the process of purification of albumin molecule from the trace concentrations of tightly bound ligands, which are contained in a commercial BSA preparation, takes place.

Carbon particles did not demonstrate cytotoxic effect towards all testing normal cell lines of different histogenesis, but DMSO, which was included into the CPs suspension as a stabilizing agent, exhibited a low cytotoxic/cytostatic effect. However, in the case of mouse bone marrow cells (MBMC), testing the carbon nanoparticles demonstrated the decrease of cytotoxic/cytostatic activity of DMSO without diminishing MBMC viability.

According to the literary data, DMSO has a cytotoxic effect as to different kinds of normal cells. This effect can be obtained by a few mechanisms. Especially, as Yuan C et al (2014) have demonstrated in the astrocytes *in vitro* model, DMSO activates apoptosis in these cells via Caspase-3 activation and suppression of the anti-apoptotic Bcl-2 protein expression [28]. At the same time, the results obtained by the Belgian research group showed that carbon nanoparticles could induce Bcl-2 expression increase and suppress Caspase-3/7 activity in the human bronchial epithelial cells [29].

Moreover, DMSO is known to disturb the cell membrane permeability (pore formation) and, through this, significantly magnify Ca^{2+} level in the cytoplasm [30]. Such distortion of the cell homeostasis is accompanied by the activation of the apoptosis or necrosis programs [31]. However, French research group has demonstrated [32] that the carbon nanoparticles are able to modify Ca^{2+} content in the cytoplasm and organelles.

These effects, probably, might be involved in the protective effect of the carbon nanoparticles shown in our mouse bone marrow model.

The visual analysis results showed that CPs did not accumulate neither in the cytoplasm nor on the membrane surface of the normal cell lines of different histogenesis. In the case of malignant human T-lymphocytes, using dark cytotoxicity method, it was found that they accumulated on their spherical surface and exhibit their cytotoxic effect.

It was also evidenced that prepared CPs suspension did not show any genotoxic effects and was absolutely safe for parenteral injection to experimental animals.

The obtained results allow asserting that suspension of highly activated CPs can be considered as an effective mean for intracorporeal treatment of the wide spectrum of diseases, where endogenous intoxication and oxidative stress play a significant role.

5. Conclusion

Our results demonstrate the possibility to obtain the stable and highly monodispersed suspension of carbon particles (1125.3 ± 243.8 nm) with a very high adsorptive potential, which is regulated by activation and grinding process conditions. The spectrophotometry, spectrofluorimetry and differential scanning microcalorimetry methods revealed the mechanism of interaction of CPs with the main transport protein of blood plasma – albumin, demonstrating the conformational shifts of the protein molecule that occur upon its contact with the surface of carbon. It was installed the dynamic type of mechanism of complexing BSA with CPs and low binding affinity between them. Highly activated CPs suspension was neither cytotoxic, nor genotoxic, did not induce acute toxicity after i.p. administration to experimental animals. Thus, it would be considered as an effective mean for intracorporeal detoxification therapy of different heavy diseases, accompanied by increasing endogenous intoxication and oxidative stress level.

Declarations

Author contribution statement

Veronika Sarnatskaya: Conceived and designed the experiments; Analyzed and interpreted the data; Wrote the paper.

Yuliia Shlapa: Analyzed and interpreted the data; Wrote the paper.

Alexandra Lykhova, Olga Brieieva, Igor Prokopenko, Serhii Solopan, Denis Kolesnik, Alexey Sidorenko: Performed the experiments.

Anatolii Belous, Vladimir Nikolaev: Analyzed and interpreted the data; Wrote the paper.

Funding statement

This work was supported by the NATO Science for Peace and Security Programme under grant 10 [G5683].

Data availability statement

Data will be made available on request.

Declaration of interests statement

The authors declare no conflict of interest.

Additional information

No additional information is available for this paper.

Acknowledgements

The appreciation for the possibility of electron microscopic studies is expressed to Dr. Maxim Kharchuk and Center for Shared Use of Danylo Zabolotny Institute of Microbiology and Virology of NAS of Ukraine.

References

[1] V.G. Nikolaev, Acceleration of regeneration processes in organs and tissues as the most important practical effect of sorption therapy with the use of activated carbons, in: Hemoperfusion, Plasmaperfusion and Other Clinical Uses of General, Boispecific, Immune and Leucocyte Adsorbents. Regenerative Medicine, Artificial Cells and Nanomedicine, World Scientific, 2017, pp. 221–243.

[2] V.G. Nikolaev, Enterosorption, in: T.M.S. Chang, H.B. Lin (Eds.), On Hemoperfusion and Artificial Organs, Academic Publishers, China, 1984, pp. 87–99.

[3] R. Sandhir, A. Yadav, A. Sunkaria, N. Singhal, Nano-antioxidants: an emerging strategy for intervention against neurodegenerative conditions, Neurochem. Int. 89 (2015) 209–226.

[4] D. Iohara, Y. Umezaki, M. Anraku, K. Uekama, F. Hirayama, In vitro and in vivo evaluation of hydrophilic C60(OH)10/2-Hydroxypropyl-β-cyclodextrin nanoparticles as an antioxidant, J. Pharm. Sci. 105 (9) (2016) 2959–2965.

[5] R. Huq, E.L. Samuel, W.K. Sikkema, L.G. Nilewski, T. Lee, M.R. Tanner, F.S. Khan, P.C. Porter, R.B. Tajhya, R.S. Patel, T. Inoue, R.G. Pautler, D.B. Corry, J.M. Tour, C. Beeton, Preferential uptake of antioxidant carbon nanoparticles by T lymphocytes for immunomodulation, Sci. Rep. 6 (2016), e33808.

[6] R. Arifa, T. Paula, M. Madeira, R. Lima, Z. Garcia, T. Ávila, V. Pinho, L. Barcelos, M. Pinheiro, L. Ladeira, K. Krambrock, M. Teixeira, D. Souza, The reduction of oxidative stress by nanocomposite Fullerol decreases mucositis severity and reverts leukopenia induced by Irinotecan, Pharmacol. Res. 107 (2016) 102–110.

[7] P.T. Bernardes, B.M. Rezende, C.B. Resende, T.P. de Paula, A.C. Reis, W.A. Gonçalves, E.G. Vieira, M.V. Pinheiro, D.G. Souza, M.G. Castor, M.M. Teixeira, V. Pinho, Nanocomposite treatment reduces disease and lethality in a murine model of acute graft-versus-host disease and preserves anti-tumor effects, PLoS One 10 (4) (2015), e0123004.

[8] X. Yang, C.J. Li, Y. Wan, P. Smith, G. Shang, Q. Cui, Antioxidative fullerol promotes osteogenesis of human adipose-derived stem cells, Int. J. Nanomed. 9 (2014) 4023–4031.

[9] M.L. Borović, I. Ičević, Z. Kanački, D. Žikić, M. Seke, R. Injac, A. Djordjević, Effects of fullerenol C60(OH)24 nanoparticles on a single-dose doxorubicin-induced cardiotoxicity in pigs: an ultrastructural study, Ultrastruct. Pathol. 38 (2) (2014) 150–163.

[10] B. Srdjenovic, V. Milic-Torres, N. Grujic, K. Stankov, A. Djordjevic, V. Vasovic, Antioxidant properties of fullerenol C60(OH)24 in rat kidneys, testes, and lungs treated with doxorubicin, Toxicol. Mech. Methods 20 (6) (2010) 298–305.

[11] G.V. Andrievsky, V.I. Bruskov, A.A. Tykhomyrov, S.V. Gudkov, Peculiarities of the antioxidant and radioprotective effects of hydrated C60 fullerene nanostuctures in vitro and in vivo, Free Radic. Biol. Med. 47 (6) (2009) 786–793.

[12] Z. Zhou, S. Joslin, A. Dellinger, M. Ehrich, B. Brooks, Q. Ren, U. Rodeck, R. Lenk, C.L. Kepley, A novel class of compounds with cutaneous wound healing properties, J. Biomed. Nanotechnol. 6 (5) (2010) 605–611.

[13] L. Xiao, K. Matsubayashi, N. Miwa, Inhibitory effect of the water-soluble polymer-wrapped derivative of fullerene on UVA-induced melanogenesis via downregulation of tyrosinase expression in human melanocytes and skin tissues, Arch. Dermatol. Res. 299 (5-6) (2007) 245–257.

[14] A. Al Faraj, A.P. Shaik, A.S. Shaik, Magnetic single-walled carbon nanotubes as efficient drug delivery nanocarriers in breast cancer murine model: noninvasive monitoring using diffusion-weighted magnetic resonance imaging as sensitive imaging biomarker, Int. J. Nanomed. 10 (2014) 157–168.
[15] A. Al Faraj, A.S. Shaik, B. Al Sayed, Preferential magnetic targeting of carbon nanotubes to cancer sites: noninvasive tracking using MRI in a murine breast cancer model, Nanomed. (Lond). 10 (6) (2015) 931–948.
[16] Q. An, C. Sun, D. Li, K. Xu, J. Guo, C. Wang, Peroxidase-like activity of Fe3O4 carbon nanoparticles enhances ascorbic acid-induced oxidative stress and selective damage to PC-3 prostate cancer cells, ACS Appl. Mater. Interfaces 5 (24) (2013) 13248–13257.
[17] W.Y. Pan, C.C. Huang, T.T. Lin, H.Y. Hu, W.C. Lin, M.J. Li, H.W. Sung, Synergistic antibacterial effects of localized heat and oxidative stress caused by hydroxyl radicals mediated by graphene/iron oxide-based nanocomposites, Nanomed 12 (2) (2016) 431–438.
[18] J. Xia, Y. Kawamura, T. Suehiro, Y. Chen, K. Sato, Carbon dots have antitumor action as monotherapy or combination therapy, Drug Discov. Ther. 13 (2) (2019) 114–117.
[19] R.J. Freshney, Culture of Animal Cells. A Manual of Basic Technique and Specialized Applications, sixth ed., John Wiley & Sons. Inc., Wiley-Blackwell, 2010, pp. 163–186.
[20] E. Vega-Avila, M.K. Pugsley, An overview of colorimetric assay methods used to assess survival or proliferation of mammalian cells, Proc. West. Pharmacol. Soc. 54 (2011) 10–14.
[21] M. Bajpayee, A. Kumar, A. Dhawan, The comet assay: a versatile tool for assessing DNA damage, in: The Comet Assay in Toxicology, 2016, pp. 1–61. Chapter I.
[22] T. Ramesh, N. Rajalakshmi, S. Dhathathreyan, Synthesis and characterization of activated carbon from jute fibers for hydrogen storage, Renew. Energy Environ. Sustain. 2 (2017) e4.
[23] B.I. Gerashchenko, O.S. Sydorenko, E.A. Snezhkova, D.O. Klymchuk, V.G. Nikolaev, Densitometry of the optically magnified dried residues representing carbon microparticles as a simple and affordable technique for determining their concentrations in aqueous suspensions, Micron 106 (2018) 42–47.
[24] X. Qi, H. Shan, Q. Zu-De, Z. Bo, H. Zhi-Ke, L. Yi, Conformation, thermodynamics and stoichiometry of HSA adsorbed to colloidal CdSe/ZnS quantum dots, Biochim. Biophys. Acta 1784 (7-8) (2008) 1020–1027.
[25] D. Gao, Y. Tian, Sh. Bi, Y. Chen, A. Yu, H. Zhang, Studies on the interaction of colloidal gold and serum albumins by spectral methods, Spectrochim. Acta Mol. Biomol. Spectrosc. 62 (4-5) (2005) 1203–1208.
[26] M. Gharagozlou, D.M. Boghaei, Interaction of water-soluble amino acid Schiff base complexes with bovine serum albumin: fluorescence and circular dichroism studies, Spectrochim. Acta Mol. Biomol. Spectrosc. 71 (2008) 1617–1622.
[27] J.R. Lakowicz, G. Weber, Quenching of fluorescence by oxygen. A probe for structural fluctuations in macromolecules, Biochem 12 (21) (1973) 4161–4170.
[28] C. Yuan, J. Gao, J. Guo, L. Bai, C. Marshall, Z. Cai, L. Wang, M. Xiao, Dimethyl sulfoxide damages mitochondrial integrity and membrane potential in cultured astrocytes, PLoS One 9 (9) (2014), e107447.
[29] M. Ghosh, S. Murugadoss, L. Janssen, S. Cokic, C. Mathyssen, K.V. Landuyt, W. Janssens, S. Carpentier, L. Godderis, P. Hoet, Distinct autophagy-apoptosis related pathways activated by Multi-walled (NM 400) and Single-walled carbon nanotubes (NIST-SRM2483) in human bronchial epithelial (16HBE14o-) cells, J. Hazard Mater. 387 (2020) 121691.
[30] O. Trubiani, E. Salvolini, R. Staffolani, R. Di Primio, L. Mazzanti, DMSO modifies structural and functional properties of RPMI-8402 cells by promoting programmed cell death, Int. J. Immunopathol. Pharmacol. 16 (3) (2003) 253–259.
[31] P. Pinton, C. Giorgi, R. Siviero, E. Zecchini, R. Rizzuto, Calcium and apoptosis: ER-mitochondria Ca2+ transfer in the control of apoptosis, Oncogene 27 (50) (2008) 6407–6418.
[32] C. Bussy, J. Cambedouzou, S. Lanone, E. Leccia, V. Heresanu, M. Pinault, M. Mayne-l'Hermite, N. Brun, C. Mory, M. Cotte, J. Doucet, J. Boczkowski, P. Launois, Carbon nanotubes in macrophages: imaging and chemical analysis by X-ray fluorescence microscopy, Nano Lett 8 (9) (2008) 2659–2663.